PNO1 promotes human cholangiocarcinoma tumorigenesis and chemosensitivity

Chuang Chen
Guangxi Cancer Hospital and Guangxi Medical University Affiliated Cancer Hospital
Shan Huang
Guangxi Cancer Hospital and Guangxi Medical University Affiliated Cancer Hospital
Guobin Wu
Guangxi Cancer Hospital and Guangxi Medical University Affiliated Cancer Hospital
Zongyu Wang
Guangxi Cancer Hospital and Guangxi Medical University Affiliated Cancer Hospital
Dongyi Lin
Guangxi Cancer Hospital and Guangxi Medical University Affiliated Cancer Hospital
Jianbo He
Guangxi Cancer Hospital and Guangxi Medical University Affiliated Cancer Hospital
Kezhi Li
Guangxi Cancer Hospital and Guangxi Medical University Affiliated Cancer Hospital
Zhiwei Han
Guangxi Cancer Hospital and Guangxi Medical University Affiliated Cancer Hospital
Xinxin Chen
Guangxi Cancer Hospital and Guangxi Medical University Affiliated Cancer Hospital
Wenxia Qiu
Guangxi Medical University First Affiliated Hospital
Yu Wang
Shandong province hospital affiliated to Shandong First Medical University
Shulei Zhao
shandong provincial hospital affiliated to Shandong first medical university
Wei Gong
shandong provincial hospital affiliated to Shandong first medical university
Shifeng Xu (shifengxu2008@163.com)
Shandong Provincial Hospital Affiliated to Shandong First Medical University

Research

Keywords: PNO1, cholangiocarcinoma, MYC, bortezomib, p53 signaling

Posted Date: January 19th, 2021

DOI: https://doi.org/10.21203/rs.3.rs-147851/v1

Abstract

Background

The partner of NOB1 homolog (PNO1) is important for ribosome biogenesis and serves as an oncogene in several cancers. However, the role of PNO1 in cholangiocarcinoma (CHOL) remains largely unknown.

Methods

The method of mRNA microarray analysis, high-throughput screening technologies, on-line databases analysis, PDXs models, biochemistry and molecular biology have been utilized to reveal the role of PNO1 in the progression of CHOL.

Results

PNO1 was significantly upregulated in CHOL tissues and predicted poor prognosis. PNO1 could induce cell proliferation and metastasis *in vitro* and *in vivo*. In CHOL cells expressing wild-type p53, PNO1 knockdown increased expression of p53 and its downstream gene p21 and decreased cell viability; these effects were blocked by p53 knockout and attenuated by the p53 inhibitor PFT-a. Furthermore, PNO1 knockdown reduced global protein synthesis and inhibiting MDM2-mediated ubiquitination and p53 degradation. Moreover, PNO1 overexpression enhanced the sensitivity to bortezomib treatment in CHOL. In addition, MYC overexpression promoted PNO1 promoter activity while MYC knockdown decreased PNO1 mRNA and protein, which led to decreased cell viability and clone formation. The expression of MYC was found positively correlated with PNO1 in CHOL patients.

Conclusions

Collectively, upregulation of PNO1 by MYC promotes cholangiocarcinoma tumorigenesis through suppressing p53 signaling pathway and enhanced the sensitivity to bortezomib treatment. PNO1 serves as a candidate of therapeutic target in CHOL treatment and clinical chemotherapy regimen.

Background

Cholangiocarcinoma is a highly malignant tumor that often arises from biliary tract epithelia. It commonly groups into intrahepatic cholangiocarcinoma (iCCA), perihilar cholangiocarcinoma (pCCA) and distal cholangiocarcinoma (dCCA) by anatomical location[1–3]. CHOL accounts for 15–20% of primary hepatobiliary malignancies, while the number of cases caused by CHOL continues to increase worldwide[4, 5]. It is mostly in the advanced stage when CHOL diagnosis is made when a patient is given a poor prognosis. Patients who are inoperable, often fail to chemotherapy and have limited of options for targeted therapy[6–8]. Therefore, exploring the underlying molecular mechanisms of CHOL development,

especially identifying novel prognostic biomarkers improve the prognosis and help to diagnosis CHOL in an early stage, is urgently needed.

Ribosome assembly factor PNO1, is also known as the RNA-binding protein “partner of NOB1”, plays an essential role in ribosome biogenesis[9–11]. It is responsible for the cleavage of 18S mediated by binding to NOB1, while its deletion could inhibit the synthesis of 18S rRNA and 40S subunit[12, 13]. In addition to the numerous studies of ribosome-related function of PNO1, several studies have reported that PNO1 acts as an oncogene in cancer cells, including colorectal cancer, lung adenocarcinoma and urinary bladder carcinoma[14–16]. Therefore, exploring the relationship between PNO1 and CHOL is essential to the future exploration of new targeted therapies.

In this study, the method of mRNA microarray analysis, high-throughput screening technologies, on-line databases analysis, PDXs models, biochemistry and molecular biology have been utilized, leading to the confirmation that PNO1 is overexpressed in CHOL tissues and MYC-mediated upregulation of PNO1 could contribute to CHOL progression by inhibiting the p53/p21 signaling pathway and enhanced the sensitivity to bortezomib treatment. Furthermore, PNO1 might act as a specific prognostic biomarker of CHOL.

Materials And Methods

Patients and tissue specimens

10 pairs of CHOL tissues (T) and para-carcinoma tissues (P) were obtained from (Shandong Provincial Hospital Affiliated to Shandong First Medical University). The para-carcinoma tissues were used for control. Tissue chips were purchased from OUTDO BIOTECH (shanghai, China). Clinicopathologic characteristics of patients could be seen in Supplementary Table S1. Samples stained with hematoxylin and eosin were verified by experienced pathologists.

Microarray analysis

Gene expression profile was detected in 10 pairs of CHOL tissues and para-carcinoma tissues, as well as in RBE cells infected with shCtrl or shPNO1 by microarray analysis. The para-carcinoma tissues and cells transfected with shCtrl were used as the control group. The RNeasy kit (Sigma) method was implied to extract the total RNA, and the concentration of which was determined by Nanodrop 2000 (Thermo Fisher Scientific). RIN value was evaluated with Agilent 2100 and Agilent RNA 6000 Nano Kit (Agilent). RNA sequencing was performed with Affymetrix human GeneChip PrimeView according to the manufacturer’s instruction, and the outcomes were scanned by Affymetrix Scanner 3000 (Affymetrix). Welch t-test with Benjamin-Hochberg FDR. was used to perform the raw data statistical significance assessment. In addition, significant difference analysis and functional analysis based on KEGG pathway enrichment analysis were executed.

Cell culture and transfection

Human cholangiocarcinoma cell lines (HuCCT1, RBE, HuH28 and TFK-1) and HEK293T were purchased from the Cell Bank of the Chinese Academy of Sciences (Shanghai, China). Human biliary epithelial cells (HIBEpiC) were obtained from Fenghbio (Hunan, China). Wild-type RBE cells (RBE/$p53^{+/+}$) and RBE cells lacking the p53 gene (RBE/$p53^{-/-}$) were produced from laboratory. HuCCT1, RBE, HuH28, TFK-1, RBE/$p53^{+/+}$ and RBE/$p53^{-/-}$ cells were grown in 90% RPMI-1640 with 10% FBS (Corning); HEK293T cells were grown in 90% DMEM with 10% FBS (Corning). Cells were grown at 37 ˚C in a humidified atmosphere of 5% CO_2. All the plasmids involved in this paper were obtained from Genechem (Shanghai, China). The information of sequences could be found in Supplementary Table S2. Cell lines in logarithmic phase were infected with lentivirus vectors with polybrene at a multiplicity of infection of 20 for 12~16 h, and then maintained in the new fresh complete medium. After 72 hours of infection, when the infection efficiency of lentivirus on cells was observed to be over 85% using fluorescence microscope (Olympus), cells were harvested for the follow-up experiments. Cells transfected with shCtrl or si-Ctrl were used as the control group.

Real-time quantitative PCR

Total RNA from the cell lines or tissue samples was isolated, respectively using TRIZOL (Sigma), reverse transcription of RNA (2.0 μg) to cDNA was performed using the PrimeScript RT reagent kit (Takara) following the manufacturer's instructions. RT-PCR was carried out using the SYBR Premix Ex Tag (Takara) on VII7 real time PCR instrument. $2^{-\Delta\Delta Ct}$ Method was used to analysis the relative quantitative of target genes with GAPDH as the internal reference. Primers for genes were synthesized by Sangon and shown in Supplementary Table S3. The para-carcinoma tissues and cells transfected with shCtrl or si-Ctrl were used as the control group.

IHC staining

Tissue sections were incubated with PNO1 antibody (1:100, Sigma) at 4°C overnight, then washed with phosphate-buffered saline (PBS) for 3 times, and incubated with horseradish peroxidase (HRP) conjugated goat anti-mouse IgG polyclonal antibody for 30 min at room temperature. DAB and hematoxylin were used to stain tissue slides. IHC scoring of patients were determined based on the combined evaluation of the staining intensity and staining extent scores. The para-carcinoma tissues were used as the control group.

Western Blotting

Cells and tissues were lysed in ice-cold RIPA buffer (Millipore) and protein concentration was detected by BCA Protein Assay Kit (HyClone-Pierce). The para-carcinoma tissues and cells transfected with shCtrl or si-Ctrl were used as the control group. The same amount of total protein from each group was separated by 12% SDS-PAGE and transferred onto a PVDF membranes (Bio-Rad Laboratory). The membranes were blocked with primary antibodies in TBST plus 5% non-fat milk. After being washed with TBST, membranes were incubated with the appropriate secondary antibody. The signals were visualized using

ECL-PLUS Kit (Amersham). Band intensities were quantified using Image J software (NIH). The information of antibodies was shown in Supplementary Table S4.

Celigo cell counting assay

72 h after the infection, cells were seeded onto a 96-well plate with the cell density of 2,000 cells/well/100 μL in RPMI-1640 medium containing 10% FBS and then further cultured for 5 days. Cells transfected with shCtrl were used as the control group. Cell counting was accomplished every day by Celigo image cytometer (Nexcelom Bioscience) and the cell proliferation curve was drawn.

CCK8 assay

Lentivirus infected CHOL cells were measured by CCK8 assay. Cells in the logarithmic phase were seeded onto 96-well plates (2,000 cells/well). CCK8 solution (10 μL, MCE) was incubated with cells for 2.5 h. The OD450 was measured by microplate reader (Tecan) and the cell viability ratio was calculated. Cells transfected with shCtrl were used as the control group.

Cell apoptosis

Infected cells were inoculated in a 6-well plate and cells were harvested when the cell density reached over 50 %. After being washed with 4°C ice-cold PBS, cells were centrifuged at 1000 rpm and resuspended with 200 μL binding buffer. Evaluation of apoptosis was performed by Annexin V-APC staining flow cytometry method (eBioscience) following the manufacturer's protocol. Cells transfected with shCtrl were used as the control group.

Cell-cycle analysis

Infected cells were inoculated in a 6-well plate and cells were harvested when the cell density reached 70 %. After being washed with 4°C ice-cold PBS, cells were centrifuged at 1000 rpm and fixed with 70% ethanol at 4°C overnight. Then the cells were washed again extensively, and then incubated with FxCycle PI/RNase Staining Solution (Thermo Fisher Scientific) for 20 minutes. DNA content was analyzed by FACS and the proportion of DNA in different phases was analyzed using FlowJo version 10.0. Cells transfected with shCtrl were used as the control group.

Colony formation assay

Lentivirus infected cells were inoculated in a 6-well plate with 800 cells/well/ 2 mL complete growth medium. Medium was exchanged every 2-3 days. Cell clones were photographed by an Olympus digital camera, then fixed and stained by 4% paraformaldehyde and Giemsa (Solarbio), respectively. The numbers of colonies were counted using photoshop 2020. Cells transfected with shCtrl were used as the control group.

Transwell migration assay

Transwell assay was performed using Corning chamber. Lentivirus infected cells were seeded in a 24-well plate with 5×10^4 cells/well the upper chambers filled with 100 μL serum-free medium. 600 μL DMEM medium plus 30% FBS were filled in the lower chamber and incubated at 37°C for 24 h (HuCCT1: 48 h). At the end of incubation, floating cells were removed and cells in lower chamber were fixed and stained with crystal violet. Images of cells were taken and analyzed using NIH image J software. Cells transfected with shCtrl were used as the control group.

Promoter activity assay

RBE cells were transduced with a plasmid expressing luciferase reporter under the control of a p53-driven promoter and lentivirus encoding anti-PNO1 or control shRNAs (the control group) for 4–6 hours. After 48 hours, cells were washed twice with PBS, and harvested with 1× PLB from the Dual-Luciferase Reporter Assay System (Promega). Then cells were lysed, centrifuged, and the supernatant was collected. Aliquots of supernatant (40 μL) were added to 96-well plates, followed by 20 μL luciferase assay reagent (Promega) at room temperature. Luciferase activity was measured immediately using a luminometer (Orion II Microplate Luminometer, Berthold Detection Systems). Data were normalized to the results obtained for the internal control Renilla luciferase.

To examine whether the 5 predicted transcription factors have indeed modulated PNO1 transcription, plasmids were constructed via encoding the full-length predicted factors. A separate plasmid was constructed encoding luciferase reporter downstream of a 2.0-kb fragment of the PNO1 promoter. Plasmid integrity was confirmed by DNA sequencing. Briefly, HEK293T or RBE cells were co-transfected with each of 5 different overexpression plasmids or MYC overexpression plasmid (500 ng), Renilla luciferase reporter (20 ng), and luciferase reporter (500 ng) using Lipofectamine 3000 Transfection reagent (Thermo Fisher Scientific). Promoter activities were measured after 48-hour transfection.

Northern blot analysis of 18S rRNA

Extracted total RNA (10 μg /sample) was fractionated on a 1.2% agarose–formaldehyde gel and transferred to Hybond NÞ membranes (Amersham). BIO-labeled probe was purchased from Thermo Fisher Scientific. The membrane was hybridized overnight in hybridization buffer (Thermo Fisher Scientific), washed twice (5 minutes each) under low-stringency conditions (2 × SSC, 0.1% SDS), blocked with blocking buffer at 50 ˚C for 30 minutes, then incubated at 50 ˚C for 20 minutes with stabilized streptavidin–horseradish peroxidase conjugate (1:300). Membranes were exposed to a phosphor storage screen and visualized using the Chemi Doc XRS_+ System (Bio-Rad). Cells transfected with shCtrl were used as the control group.

Ribosome profile analysis

Transfected RBE cells were treated with 100 μg/mL cycloheximide for 15 minutes, washed with ice-cold PBS containing 100 μg/mL cycloheximide, and then resuspended in hypotonic buffer [10 mmol/L HEPES (pH 7.9), 1.5 mmol/L $MgCl_2$, 10 mmol/L KCl, 0.5 mmol/L dithiothreitol (DTT), 100 μg/mL cycloheximide,

40 U/mL RNase inhibitor, 1 × protease inhibitor cocktail]. Cells were centrifuged at 14,000 rpm for 15 minutes at 4 ˚C. Total protein (1 mg) was loaded onto a linear sucrose gradient (5%–50%) and centrifuged for 3 hours at 38,000 rpm at 4 ˚C. Cells transfected with shCtrl were used as the control group.

Protein synthesis assay

Global protein synthesis was assayed using a commercial kit (Cayman Chemical). Transfected RBE cells were incubated for 30 minutes with o-propargyl-puromycin in complete medium in 96-well plates (100 µL/well). Cells transfected with si-Ctrl were used as the control group. Cells were fixed with cell-based assay fixative (100 µL/well), stained with 5 FAM-azide (Cayman Chemical), and photographed under a fluorescence microscope (Accu-Scope). Images were collected using MetaMorph image acquisition software (Molecular Devices). Fluorescence intensity in single cells was quantitated using Image Pro Plus software (Media Cybernetics).

Xenograft tumor studies

All animal procedures were carried out in accordance with the Helsinki Declaration and were approved by the Ethics Committee of Shandong Provincial Hospital Affiliated to Shandong First Medical University (NO.2019-156). For cell line tumor xenografts, 0.2 mL exponentially growing lentivirus infected HuCCT1 cell suspensions at a destiny of 2× 10^7cell/ml were injected subcutaneously into BALB/c nude mice (4-6 weeks old). For metastasis mouse models, 0.1 ml lentivirus infected HuCCT1 cell suspensions at a destiny of 1× 10^7 cell/ml were injected intravenously into BALB/c nude mice (4-6 weeks old). For the PDX model, tumor tissues were obtained directly from the operating room, dissected carefully, trimmed into small pieces (approximately 2~3-mm^3) under sterile conditions and implanted subcutaneously into the flanks of female NOD/SCID mice. After 2 months of tumor growth, the established PDX tumors were transplanted subcutaneously into the flanks of female NOD/SCID mice. When the tumors reached about 100 mm^3, the mice received an intraperitoneal dose of bortezomib (0.5 mg/kg, twice a week) for bortezomib treatment, and the normal group were treated with Saline for comparison at the same time. Tumor growth was assessed twice a week using a caliper and tumor volumes (V) were estimated as $V=\pi/6\times L\times W\times W$ (L and W was tumor length and width, respectively). Mice were sacrificed at humane endpoints and the tumor tissues were removed for immunostaining.

Ki-67 staining assay

Tissue slides were blocked with 3% PBS-H_2O_2 and were incubated with primary antibody Ki-67 at 4°C overnight. Then slides were incubated with HRP goat anti-rabbit IgG at room temperature for 2 h. Finally, all slides were stained by Hematoxylin (# BA4041, Baso) and Eosin (# BA4022, Baso). Tumors transfected with shCtrl were used as the control group.

Statistical Analysis

Student's T-Test and one-way ANOVA were used to analyze the statistical significance. All statistical analysis was performed using SPSS 22.0 (IBM, SPSS) and GraphPad Prism 8.01 (GraphPad Software). Each bar represents the mean values ± SD of three independent experiments. $P < 0.05$ was considered statistically significant. Kaplan-Meier survival analysis was performed using the log-rank test. The primary endpoint of the animal study was defined as the tumor growth, tumor volumes and KI67 expression in tumor tissues.

Results

Identification of PNO1 as a novel target in CHOL

At present study, we first utilized 10 pairs of CHOL tissues and non-tumorous bile ducts tissues for microarray analysis, which revealed 2,394 upregulated DEGs and 1,562 downregulated DEGs (Figure 1A and 1B). To identify potential oncogenes, we selected 20 up-regulated DEGs that have not been reported in CHOL-related study (Figure 1C). Using high-content screening, we have detected cell growth and the knockdown expression of selected genes in RBE cells with lentivirus-transduced target-shRNA (Supplementary Figure S1A). The results suggested that cell growth was distinctly inhibited in sh*SYT13, shCDCA5, shTMED3, shPNO1* and sh*DEPDC1* groups (Figure 1D-F). Considering the most obvious inhibitory effects of PNO1 knockdown, PNO1 was selected for subsequent studies.

PNO1 is upregulated in CHOL tissue samples and predicts poor prognosis

To further evaluate the expression pattern of PNO1 in CHOL, the protein expression of PNO1 in 83 CHOL tissues and 31 para-carcinoma tissues were measured using IHC. The results showed that PNO1 was significantly upregulated in tumor tissues (Figure 1G and 1H). Based on detailed tumor characteristics information from the CHOL patients, we found that high expression of PNO1 was positively correlated with advanced pathological grading, TNM stage, recurrence patients and poor prognosis of CHOL patients (Figure 1I-L). The PNO1 mRNA expression levels were also confirmed in CHOL by RT-PCR (Figure 1M). The results suggested that PNO1 might serve as an oncogenic role in CHOL tumor tumorigenesis.

PNO1 promotes CHOL cell proliferation and migration in vitro.

PNO1 is highly expressed in cultured CHOL cell lines (HuCCT1, RBE, HuH28 and TFK-1), compared to normal bile duct epithelial cell line HIBEpic (Supplementary Figure S1B). The decreased of PNO1 mRNA expression in three shRNA or si-RNA (PNO1-target) suggested successful transfection, and shPNO1-1 was selected for subsequent research because of its most effective interference verified by CCK8 assay in RBE cells (Supplementary Figure S1C-E). In cultured HuCCT1 and RBE cells, the downregulation of both PNO1 protein and mRNA levels were verified (Figure 2A), and the inhibition effects of shPNO1 on cell proliferation and migration were confirmed, including decreased in cell viability (Figure 2B), percentage of cells in S phase (Figure 2C), colony formation (Figure 2E) and chemotaxis cells (Figure 2F), and also inducing the percentage of cells to undergo apoptosis (Figure 2D). On the contrary, the upregulation of

PNO1 in HuH28 and TFK-1 cells could increase cell viability, colony formation and chemotaxis cells (Figure 2G-J).

PNO1 knockdown inhibits CHOL tumorigenesis in vivo

Mice xenograft models were used through subcutaneous injection of HuCCT1 cell models to verify the effect of PNO1 knockdown on tumor growth in vivo. We selected a small sample size (n=10), because initial intention was to gather basic evidence regarding the role of PNO1 in CHOL in more complex experimental designs. The measurement of tumor volume started at day 11 post tumor-inoculation and end up with day 32. The results of which illustrated a lower tumor weight and significantly smaller tumor size compared with controls (Figure 3A-C). Moreover, Ki-67 staining was used to detect proliferative activity of tumors, which was shown to be significantly weaker in shPNO1 group than shCtrl group (Figure 3D). The result also showed the expression of PNO1 at the mRNA level in tumors (Figure 3E). In addition, metastasis mouse models by intravenous injection were established. After six weeks, the mice were sacrificed and the lung, liver, organ in gastrointestinal tract were harvested. We found that PNO1 downregulation HuCCT1 cells formed fewer lung and liver metastatic nodules by a Living Image System (Figure 3F).

Oncogenic activities of PNO1 depend on p53/p21 signaling

To further explore the mechanism of PNO1 on CHOL development, microarray analysis was performed to determine DEGs in RBE cells transduced with lentivirus encoding either shPNO1 or shCtrl and revealed 2,083 upregulated DEGs and 1,805 downregulated DEGs (Figure 4A and 4B). Combined with KEGG pathway enrichment analysis, the results indicated that PNO1 may participate in several functional pathways involved in cell proliferation and migration (Figure 4C). The expression of 15 selected DEGs from the 10 most enriched signaling pathways were consistent with the microarray analysis and p53 was the most strongly upregulated gene in response to PNO1 knockdown by RT-PCR (Figure 4D). Furthermore, the analysis of STRING database indicated that p53 could bind to other 14 DEGs and may be the most potential effector of PNO1 in CHOL (Figure 4E). Indeed, we demonstrated that PNO1 knockdown increased luciferase activity in the p53-driven luciferase reporter assay (Figure 4F). Western blot analysis confirmed increased protein expression of both p53 and p21 (Figure 4G). The inhibitory effects of PNO1 knockdown were prevented when p53 was knocked out (Figure 4H and I), and the inhibitory effects were attenuated when cells were treated with the p53 inhibitor PFT-a (Figure 4J).

PNO1 knockdown activates p53 by inhibiting MDM2-mediated ubiquitination and degradation of p53

RNA profiling and Northern blotting verified that PNO1 knockdown in RBE cells significantly decreased amounts of 18S rRNA (Figure 5A), 40S and 60S subunits, and the 80S ribosome (Figure 5B). Protein synthesis assay showed that PNO1 knockdown in RBE cells visibly inhibited of global protein synthesis (Figure 5C). Western blot analysis and coimmunoprecipitation (co-IP) assay indicated that PNO1 knockdown led to a reduction in degradation of p53 (Figure 5D) and ubiquitination of p53 (Figure 5E).

Moreover, co-IP analysis indicated that PNO1 knockdown increased the binding of RPL11 to MDM2(Figure 5F).

PNO1 facilitates the therapeutic effect of bortezomib in CHOL

Meanwhile, we found that PNO1 knockdown in RBE cells could increase the protein level of PTEN while overexpression of PNO1 could reduce the expression of PTEN (Figure 6A). In addition, co-IP analysis indicated that PNO1 knockdown increased the binding of p53 to PTEN (Figure 6B). It has been reported that PTEN attenuated bortezomib efficacy in CHOL treatment[17]. To explore the effect of manipulating PNO1 abundance on sensitivity to bortezomib, cell models in vitro and PDXs models in vivo were established. As shown in CCK8 assays, RBE cell viability was inhibited by 0.5 μM concentration of bortezomib when compared with saline, whereas an enhanced therapeutic effect was discovered upon PNO1 overexpression (Figure 6C). Immunohistochemistry (IHC) staining revealed low expression of PNO1 and concurrent up-regulation of p53 and PTEN expression in tumor tissues from CC1 when compared with CC2 (Figure 6D). Consistent with the in vitro findings, bortezomib treatment was effective at limiting tumor growth in PNO1-high expression PDXs when compared with PNO1-low expression PDXs (Figure 6E and 6F).

Transcription factor MYC positively regulates PNO1 expression in CHOL

To explore the upstream mechanism of PNO1 on CHOL, we identified MYC as an important transcription factor of PNO1 using TFBIND screening of transcription factor binding sites combined with DEGs from mRNA microarray analysis of RBE cells (Figure 7A-C). We found that MYC knockdown distinctly decreased expression levels of PNO1 mRNA and protein in RBE cells (Figure 7D and 7E), while also inducing the mRNA expression of p53 and p21. Moreover, MYC knockdown in RBE cells visibly decreased cell viability and colony formation (Figure 7F and 7G). In addition, MYC knockdown also induced cell cycle arrest and cell apoptosis (Figure 7H and 7I). The result demonstrated that MYC was highly expressed in CHOL tissues and was positively correlated with PNO1 based on data from on-line GEPIA2 (Figure 7J and 7H). All of the above results led to the suggestion that MYC overexpression may help drive CHOL by triggering PNO1 overexpression.

Discussion

Several past studies have confirmed PNO1 as an oncogene in tumorigenic processes. For example, Peng revealed that mammalian PNO1 worked as a ribosome assembly factor in colorectal cancer cells, and its oncogenic effects could serve as a novel therapeutic strategy in colorectal cancer[14]. Guo offered the evidence that PNO1, a direct functional target of miR-340-5p, was related with Notch pathway and EMT, which acts as promising target for the treatment of lung adenocarcinoma in the future[16]. In the present study, we found that PNO1 was upregulated in CHOL tissues and knockdown the expression of PNO1 could inhibit RBE cell growth in vitro, which might be predictive of the potential of PNO1 as a prognostic biomarker and its oncogenic effects in CHOL progression.

To further confirm the expression pattern of PNO1 in CHOL, we detected the PNO1 protein levels of 83 CHOL clinical samples by IHC staining. Indeed, these results were consistent with the previous mRNA microarray analysis: PNO1 was upregulated in CHOL tissues. Moreover, based on tissue microarray analysis, high PNO1 expression was positively correlated with tumor grade and poor survival of patients with CHOL. These results highlighted the potential of PNO1 as a prognostic biomarker and its oncogenic effects in CHOL progression.

In our study, we demonstrated that PNO1 was significantly upregulated in CHOL cell lines. The knockdown of PNO1 repressed cell growth, colony formation, cell migration, induced cell cycle arrest, cell apoptosis, and also inhibited tumor growth and metastasis in vivo and vitro. On the contrary, overexpression of PNO1 promoted cell proliferation and migration. The tumor suppressor effects of PNO1 knockdown had been previously reported in cell cultures, and this is the first work in which the suppressor activity of shPNO1 is reported for in xenograft models in vivo. Our findings may result in extrapolating our results to humans and showing a promising field of research emerges in the area of CHOL. These results suggested that PNO1 might serve as a potential target molecule in CHOL patients.

Subsequently, we explored the possible mechanism of oncogenic function of PNO1 using mRNA microarray analysis. Based on the DEGs between RBE cells treated with shPNO1 or shCtrl, KEGG pathway enrichment analysis was used to identify the possible functional pathways. The results showed that PNO1 could possibly participate in several functional pathways involved in cell cycle progression, cell proliferation and metastasis. The mRNA levels of selected DEGs involved in the 10 most enrichment signaling pathway were consistent with the mRNA microarray analysis by RT-PCR. Combined with the result from the STRING database, we focused on the function of p53 at the follow-up study. It is known that tumor suppressor p53 involved in a variety of cellular events, for instance, p53/p21 signaling could induce cell cycle arrest and apoptosis as well as repress cell proliferation; oncogenes could promote MDM2-mediated degradation and ubiquitination of p53[18–29]. In our study, we confirmed that the knockdown of PNO1 could increase luciferase activity by a p53-driven luciferase reporter assay and could enhance the protein levels of p53, CDKN1A (p21) and MDM2. Moreover, the knockout of p53 or the addition of p53 inhibitor PFT-a could enhance cell viability, which could be reduced by the knockdown of PNO1.

It was well known the role of ribosome biogenesis in the control of a cell to synthesize proteins and hence acts an essential role in cell proliferation and migration, which was associated with many diseases including cancer[30–32]. In the present study, we found that PNO1 knockdown in RBE cells decreased the amounts of 18S rRNA, 40S subunits, 60S subunits, and the 80S ribosome, which led to significant inhibition of global protein synthesis by RNA profiling and Northern blotting. Meanwhile, a p53-driven luciferase reporter assay and quantitative PCR analysis indicated that PNO1 knockdown could increase luciferase activity and p53 mRNA expression, while also leading to a decrease in the degradation and ubiquitination of p53. The results suggested that PNO1 knockdown could activate p53 signaling. It has been revealed that ribosome protein RPL11 binds to MDM2 and inhibits its ubiquitin ligase activity toward p53, resulting in p53 accumulation[18, 20, 30, 33–38]. We confirmed that PNO1 knockdown

distinctly increased the binding of RPL11 to MDM2, suggesting that ribosomal stress increased the binding of RPL11 to MDM2 and decreased ubiquitination and degradation of p53, which may contribute to the accumulation of p53.

In addition, results from cell models and patient-derived xenografts (PDX) models indicated that PNO1 overexpression enhanced the therapeutic effect for BZ in CHOL. Meanwhile, one rejoices in surprise realizing that PNO1 deficient caused a significant increase in protein levels of PTEN and p53 in vivo. A previous study reported that PTEN inhibited proteasome activity and attenuated bortezomib efficacy in CHOL [39]. PTEN might modulate the function of proteasomes [40]. In our study, PNO1 knockdown suppressed ubiquitin degradation of p53. As well know that The *PTEN* and *p53* tumor suppressors are among the most commonly inactivated or mutated genes in human cancer [41]. Of note, the p53 protein cooperates with PTEN and might be an essential blockage in development of many tumors [42]. Collectively, we guessed that knockdown of PNO1 elevated PTEN/p53 expression and then depressed the therapeutic effect for BZ in CHOL.

Indeed, MYC could act as a regulator of ribosome biogenesis and an important target for cooperative actions of p53 and PTEN in the regulation of tumor development [43–45]. In our study, MYC was identified as a potential transcription factor of PNO1. We suggested that MYC knockdown reduced expression levels of PNO1 mRNA and protein in RBE cells, while also increasing the levels of p53and p21. Furthermore, MYC knockdown in RBE cells visibly reduced cell viability and induced cell cycle arrest as well as cell apoptosis. We also identified that MYC expression was positively correlated with PNO1 based on on-line CHOL databases analysis. These results suggested that MYC overexpression may contribute to driving CHOL via triggering PNO1 overexpression, which was consistent with previous studies stating that MYC was an oncogene in cancers[46–48]. However, detailed mechanism of how MYC regulates PNO1 expression needs to be explored through further studies.

Conclusions

In conclusion, our study identified PNO1 as a tumor promotor in CHOL, which could be possibly used as a prognostic indicator and novel therapeutic target in the treatment of CHOL. We found that PNO1 was upregulated in CHOL tissues and its upregulation or downregulation could promote or suppress the development and progression of CHOL respectively. Furthermore, our results provided evidence that PNO1 could be regulated by transcription factor MYC, and its oncogenic effects were regulated by p53 signaling pathway. Our findings also revealed that the relationship between PNO1/PTEN/p53 axis and bortezomib sensitivity in CHOL treatment. These findings highlighted the potential of PNO1 as a novel targeted therapy in CHOL.

Abbreviations

ANOVA, analysis of variance; CCK-8, cell counting kit-8; DEGs, differentially expressed genes; IHC, immunohistochemistry; IVIS, *in vivo* imaging system; KEGG, Kyoto Encyclopedia of Genes and Genomes;

RT-PCR, real time polymerase chain reaction; SDS-PAGE, sodium dodecyl sulfate polyacrylamide gel electrophoresis; shRNA, short hairpin RNA; shCtrl, short hairpin RNA of control; TMA, tissue microarray; PBS, phosphate-buffered saline; PLB, Passive Lysis Buffer; BZ, bortezomib

Declarations

Acknowledgments

We would like to thank the Shandong Provincial Hospital Affiliated to Shandong First Medical University.

Authors' contributions

S.F.X., C.C. and S.H. conceived the project, designed experiments, analysed data, and wrote the paper. K.Z.L., Z.W.H., X.X.C., W.X.Q., Z.Y.W., D.Y.L. and S.L.Z. performed experiments and collected data. G.B.W., J.B.H., Y.W. and W.G. interpreted data and revised the paper. All authors critically reviewed the paper and had final approval of it.

Ethics approval and consent to participate

All animal experiments in our study were carried out in accordance with the Helsinki Declaration, and approved by the Ethics Committee of Shandong Provincial Hospital Affiliated to Shandong First Medical University (NO.2019-156). Patients were informed that the resected specimens were stored by the hospital and potentially used for scientific research, and that their privacy would be maintained. All patients provided informed consent prior to undergoing screening procedures. Our study protocol (NO.2019-156) was approved by the Ethics Committee of Shandong Provincial Hospital Affiliated to Shandong First Medical University.

Consent for publication

Not applicable.

Data availability

The datasets generated and/or analyzed during the current study are not publicly available but are available from the corresponding author on reasonable request.

Conflict of interest

The authors declare no conflict of interest.

Funding information

This study was supported by Key R & D project of Shandong Province (2016GGB14064, 2019GSF108231) and Science and technology development project of Jinan City (201907073).

References

1. Forner A, Vidili G, Rengo M, Bujanda L, Ponz-Sarvise M, Lamarca A: **Clinical presentation, diagnosis and staging of cholangiocarcinoma**. *Liver Int* 2019, **39 Suppl 1**:98-107.
2. Mahipal A, Tella SH, Kommalapati A, Anaya D, Kim R: **FGFR2 genomic aberrations: Achilles heel in the management of advanced cholangiocarcinoma**. *Cancer Treat Rev* 2019, **78**:1-7.
3. Chu KJ, Ma YS, Jiang XH, Wu TM, Wu ZJ, Li ZZ, Wang JH, Gao QX, Yi B, Shi Y *et al*: **Whole-Transcriptome Sequencing Identifies Key Differentially Expressed mRNAs, miRNAs, lncRNAs, and circRNAs Associated with CHOL**. *Mol Ther Nucleic Acids* 2020, **21**:592-603.
4. Khan SA, Tavolari S, Brandi G: **Cholangiocarcinoma: Epidemiology and risk factors**. *Liver Int* 2019, **39 Suppl 1**:19-31.
5. Loeffler MA, Hu J, Kirchner M, Wei X, Xiao Y, Albrecht T, De La Torre C, Sticht C, Banales JM, Vogel MN *et al*: **miRNA profiling of biliary intraepithelial neoplasia reveals stepwise tumorigenesis in distal cholangiocarcinoma via the miR-451a/ATF2 axis**. *J Pathol* 2020.
6. Jang SI, Fang S, Baek YY, Lee DH, Na K, Lee SY, Lee DK: **Local Delivery of Gemcitabine Inhibits Pancreatic and Cholangiocarcinoma Tumor Growth by Promoting Epidermal Growth Factor Receptor Degradation**. *Int J Mol Sci* 2020, **21**(5).
7. Kelley RK, Bridgewater J, Gores GJ, Zhu AX: **Systemic therapies for intrahepatic cholangiocarcinoma**. *J Hepatol* 2020, **72**(2):353-363.
8. Wang J, Xing X, Li Q, Zhang G, Wang T, Pan H, Li D: **Targeting the FGFR signaling pathway in cholangiocarcinoma: promise or delusion?***Ther Adv Med Oncol* 2020, **12**:1758835920940948.
9. Wang X, Wu T, Hu Y, Marcinkiewicz M, Qi S, Valderrama-Carvajal H, Luo H, Wu J: **Pno1 tissue-specific expression and its functions related to the immune responses and proteasome activities**. *PLoS One* 2012, **7**(9):e46093.
10. Zhou GJ, Zhang Y, Wang J, Guo JH, Ni J, Zhong ZM, Wang LQ, Dang YJ, Dai JF, Yu L: **Cloning and characterization of a novel human RNA binding protein gene PNO1**. *DNA Seq* 2004, **15**(3):219-224.
11. Miura M, Hirose M, Miwa T, Kuwae S, Ohi H: **Cloning and characterization in Pichia pastoris of PNO1 gene required for phosphomannosylation of N-linked oligosaccharides**. *Gene* 2004, **324**:129-137.
12. Turowski TW, Lebaron S, Zhang E, Peil L, Dudnakova T, Petfalski E, Granneman S, Rappsilber J, Tollervey D: **Rio1 mediates ATP-dependent final maturation of 40S ribosomal subunits**. *Nucleic Acids Res* 2014, **42**(19):12189-12199.
13. Scaiola A, Pena C, Weisser M, Bohringer D, Leibundgut M, Klingauf-Nerurkar P, Gerhardy S, Panse VG, Ban N: **Structure of a eukaryotic cytoplasmic pre-40S ribosomal subunit**. *EMBO J* 2018, **37**(7).
14. Shen A, Chen Y, Liu L, Huang Y, Chen H, Qi F, Lin J, Shen Z, Wu X, Wu M *et al*: **EBF1-Mediated Upregulation of Ribosome Assembly Factor PNO1 Contributes to Cancer Progression by Negatively Regulating the p53 Signaling Pathway**. *Cancer Res* 2019, **79**(9):2257-2270.
15. Lin C, Yuan H, Wang W, Zhu Z, Lu Y, Wang J, Feng F, Wu J: **Importance of PNO1 for growth and survival of urinary bladder carcinoma: Role in core-regulatory circuitry**. *J Cell Mol Med* 2020,

24(2):1504-1515.

16. Liu D, Lin L, Wang Y, Chen L, He Y, Luo Y, Qi L, Guo Y, Chen L, Han Z *et al*: **PNO1, which is negatively regulated by miR-340-5p, promotes lung adenocarcinoma progression through Notch signaling pathway**. *Oncogenesis* 2020, **9**(5):58.
17. Jiang TY, Pan YF, Wan ZH, Lin YK, Zhu B, Yuan ZG, Ma YH, Shi YY, Zeng TM, Dong LW *et al*: **PTEN status determines chemosensitivity to proteasome inhibition in cholangiocarcinoma**. *Sci Transl Med* 2020, **12**(562).
18. Horie S, Endo K, Kawasaki H, Terada T: **Overexpression of MDM2 protein in intrahepatic cholangiocarcinoma: relationship with p53 overexpression, Ki-67 labeling, and clinicopathological features**. *Virchows Arch* 2000, **437**(1):25-30.
19. Vousden KH, Prives C: **Blinded by the Light: The Growing Complexity of p53**. *Cell* 2009, **137**(3):413-431.
20. Kaindl U, Morak M, Portsmouth C, Mecklenbrauker A, Kauer M, Zeginigg M, Attarbaschi A, Haas OA, Panzer-Grumayer R: **Blocking ETV6/RUNX1-induced MDM2 overexpression by Nutlin-3 reactivates p53 signaling in childhood leukemia**. *Leukemia* 2014, **28**(3):600-608.
21. Kastenhuber ER, Lowe SW: **Putting p53 in Context**. *Cell* 2017, **170**(6):1062-1078.
22. Lopes EA, Gomes S, Saraiva L, Santos MMM: **Small Molecules Targeting Mutant P53: A Promising Approach for Cancer Treatment**. *Curr Med Chem* 2019, **26**(41):7323-7336.
23. Cen B, Lang JD, Du Y, Wei J, Xiong Y, Bradley N, Wang D, DuBois RN: **Prostaglandin E2 Induces miR675-5p to Promote Colorectal Tumor Metastasis via Modulation of p53 Expression**. *Gastroenterology* 2020, **158**(4):971-984 e910.
24. Deng L, Yao P, Li L, Ji F, Zhao S, Xu C, Lan X, Jiang P: **p53-mediated control of aspartate-asparagine homeostasis dictates LKB1 activity and modulates cell survival**. *Nat Commun* 2020, **11**(1):1755.
25. Duffy MJ, Synnott NC, O'Grady S, Crown J: **Targeting p53 for the treatment of cancer**. *Semin Cancer Biol* 2020.
26. Li X, Guo M, Cai L, Du T, Liu Y, Ding HF, Wang H, Zhang J, Chen X, Yan C: **Competitive ubiquitination activates the tumor suppressor p53**. *Cell Death Differ* 2020, **27**(6):1807-1818.
27. Lu C, Jiang W, Hui B, Rong D, Fu K, Dong C, Tang W, Cao H: **The circ_0021977/miR-10b-5p/P21 and P53 regulatory axis suppresses proliferation, migration, and invasion in colorectal cancer**. *J Cell Physiol* 2020, **235**(3):2273-2285.
28. Tiwari A, Tashiro K, Dixit A, Soni A, Vogel K, Hall B, Shafqat I, Slaughter J, Param N, Le A *et al*: **Loss of HIF1A From Pancreatic Cancer Cells Increases Expression of PPP1R1B and Degradation of p53 to Promote Invasion and Metastasis**. *Gastroenterology* 2020.
29. Xu CL, Sang B, Liu GZ, Li JM, Zhang XD, Liu LX, Thorne RF, Wu M: **SENEBLOC, a long non-coding RNA suppresses senescence via p53-dependent and independent mechanisms**. *Nucleic Acids Res* 2020, **48**(6):3089-3102.

30. Deisenroth C, Zhang Y: **Ribosome biogenesis surveillance: probing the ribosomal protein-Mdm2-p53 pathway**. *Oncogene* 2010, **29**(30):4253-4260.
31. Pelletier J, Thomas G, Volarevic S: **Ribosome biogenesis in cancer: new players and therapeutic avenues**. *Nat Rev Cancer* 2018, **18**(1):51-63.
32. Prakash V, Carson BB, Feenstra JM, Dass RA, Sekyrova P, Hoshino A, Petersen J, Guo Y, Parks MM, Kurylo CM *et al*: **Ribosome biogenesis during cell cycle arrest fuels EMT in development and disease**. *Nat Commun* 2019, **10**(1):2110.
33. Zheng J, Lang Y, Zhang Q, Cui D, Sun H, Jiang L, Chen Z, Zhang R, Gao Y, Tian W *et al*: **Structure of human MDM2 complexed with RPL11 reveals the molecular basis of p53 activation**. *Genes Dev* 2015, **29**(14):1524-1534.
34. Lu J, McEachern D, Li S, Ellis MJ, Wang S: **Reactivation of p53 by MDM2 Inhibitor MI-77301 for the Treatment of Endocrine-Resistant Breast Cancer**. *Mol Cancer Ther* 2016, **15**(12):2887-2893.
35. Kayama K, Watanabe S, Takafuji T, Tsuji T, Hironaka K, Matsumoto M, Nakayama KI, Enari M, Kohno T, Shiraishi K *et al*: **GRWD1 negatively regulates p53 via the RPL11-MDM2 pathway and promotes tumorigenesis**. *EMBO Rep* 2017, **18**(1):123-137.
36. de Oliveira Ribeiro H, Cortez AP, de Avila RI, da Silva ACG, de Carvalho FS, Menegatti R, Liao LM, Valadares MC: **Small-molecule MDM2 inhibitor LQFM030-induced apoptosis in p53-null K562 chronic myeloid leukemia cells**. *Fundam Clin Pharmacol* 2020.
37. Wang Z, Zhan Y, Xu J, Wang Y, Sun M, Chen J, Liang T, Wu L, Xu K: **beta-Sitosterol Reverses Multidrug Resistance via BCRP Suppression by Inhibiting the p53-MDM2 Interaction in Colorectal Cancer**. *J Agric Food Chem* 2020, **68**(12):3850-3858.
38. Xie X, He G, Siddik ZH: **Cisplatin in Combination with MDM2 Inhibition Downregulates Rad51 Recombinase in a Bimodal Manner to Inhibit Homologous Recombination and Augment Tumor Cell Kill**. *Mol Pharmacol* 2020, **97**(4):237-249.
39. Jiang T-Y, Pan Y-F, Wan Z-H, Lin Y-K, Zhu B, Yuan Z-g, Ma Y-H, Shi Y-Y, Zeng T-M, Dong L-W *et al*: **PTEN status determines chemosensitivity to proteasome inhibition in cholangiocarcinoma**. *Science Translational Medicine* 2020, **12**(562):eaay0152.
40. He X, Arrotta N, Radhakrishnan D, Wang Y, Romigh T, Eng C: **Cowden syndrome-related mutations in PTEN associate with enhanced proteasome activity**. *Cancer Res* 2013, **73**(10):3029-3040.
41. Dong J-T: **Prevalent mutations in prostate cancer**. *Journal of Cellular Biochemistry* 2006, **97**(3):433-447.
42. Nakanishi A, Kitagishi Y, Ogura Y, Matsuda S: **The tumor suppressor PTEN interacts with p53 in hereditary cancer (Review)**. *Int J Oncol* 2014, **44**(6):1813-1819.
43. Zheng H, Ying H, Yan H, Kimmelman AC, Hiller DJ, Chen A-J, Perry SR, Tonon G, Chu GC, Ding Z *et al*: **p53 and Pten control neural and glioma stem/progenitor cell renewal and differentiation**. *Nature* 2008, **455**(7216):1129-1133.
44. van Riggelen J, Yetil A, Felsher DW: **MYC as a regulator of ribosome biogenesis and protein synthesis**. *Nat Rev Cancer* 2010, **10**(4):301-309.

45. Morcelle C, Menoyo S, Moron-Duran FD, Tauler A, Kozma SC, Thomas G, Gentilella A: **Oncogenic MYC Induces the Impaired Ribosome Biogenesis Checkpoint and Stabilizes p53 Independent of Increased Ribosome Content**. *Cancer Res* 2019, **79**(17):4348-4359.
46. He J, Gerstenlauer M, Chan LK, Leithauser F, Yeh MM, Wirth T, Maier HJ: **Block of NF-kB signaling accelerates MYC-driven hepatocellular carcinogenesis and modifies the tumor phenotype towards combined hepatocellular cholangiocarcinoma**. *Cancer Lett* 2019, **458**:113-122.
47. Ganci F, Pulito C, Valsoni S, Sacconi A, Turco C, Vahabi M, Manciocco V, Mazza EMC, Meens J, Karamboulas C *et al*: **PI3K Inhibitors Curtail MYC-Dependent Mutant p53 Gain-of-Function in Head and Neck Squamous Cell Carcinoma**. *Clin Cancer Res* 2020, **26**(12):2956-2971.
48. Olivero CE, Martinez-Terroba E, Zimmer J, Liao C, Tesfaye E, Hooshdaran N, Schofield JA, Bendor J, Fang D, Simon MD *et al*: **p53 Activates the Long Noncoding RNA Pvt1b to Inhibit Myc and Suppress Tumorigenesis**. *Mol Cell* 2020, **77**(4):761-774 e768.

Figures

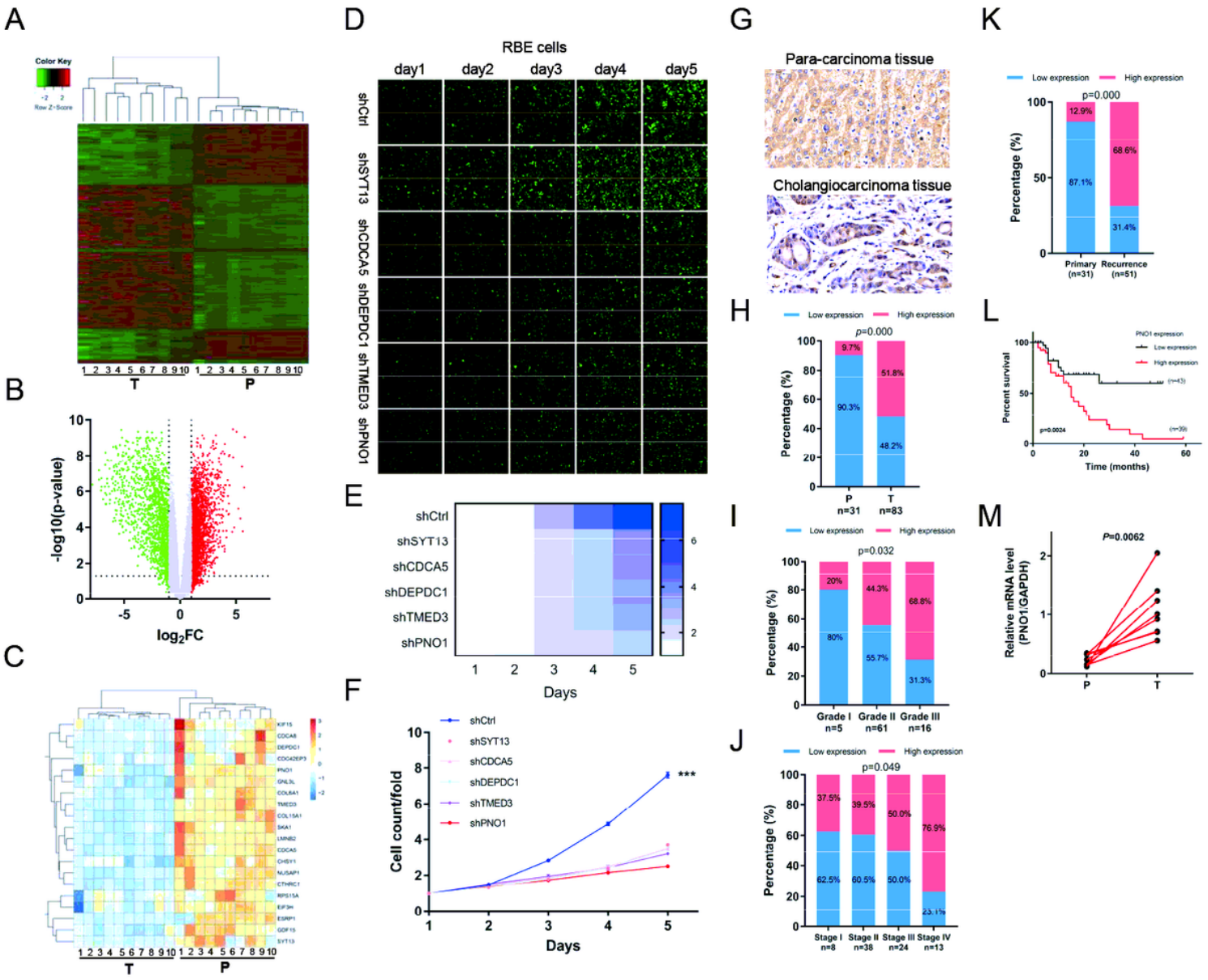

Figure 1

PNO1 is a specific prognostic biomarker in CHOL tissues. mRNA microarray analysis was used to identify DEGs between 10 pairs of CHOL tissues (T) and adjacent normal tissues (N). High-content screening and lentivirus-delivered, shRNA-targeted of indicated genes, were used to detect the effects of 20selected genes on CHOL cell growth. (A and B) Clustering Heatmap (A) and volcano plots (B) were used to show the DEGs from mRNA microarray analysis (|Log2FC| > 1, adjusted p-value < 0.05). (C) Heatmap of 20 selected DEGs. (D) Effects of 20 selected DEGs on growth of RBE cells, infected with shCtrl or target-shRNA (50 μm). (E and F) Heatmap(E) and growth curves (F) showing the growth of RBE cells. Data were normalized to cell number on day 1 and are represented as fold change. ***, P < 0.001, compared with shCtrl. (G) Representative images of para-carcinoma tissues and CHOL tissues showing PNO1 expression (50 μm). (H) PNO1 protein levels in 83 CHOL tissues and 31 para-carcinoma tissues were determined by IHC. (I) Correlation analysis between the PNO1 IHC score and tumor Grade. (J) Correlation analysis between the PNO1 IHC score and tumor TNM stage. (K) Correlation analysis between the PNO1 IHC score

and tumor recurrence. (L) Kaplan–Meier survival curve analysis showing the correlation between the PNO1 IHC score and OS in CHOL patients. (M) RT-PCR showing PNO1 mRNA levels between 10 pairs CHOL tissues (T) and para-carcinoma tissues (P).

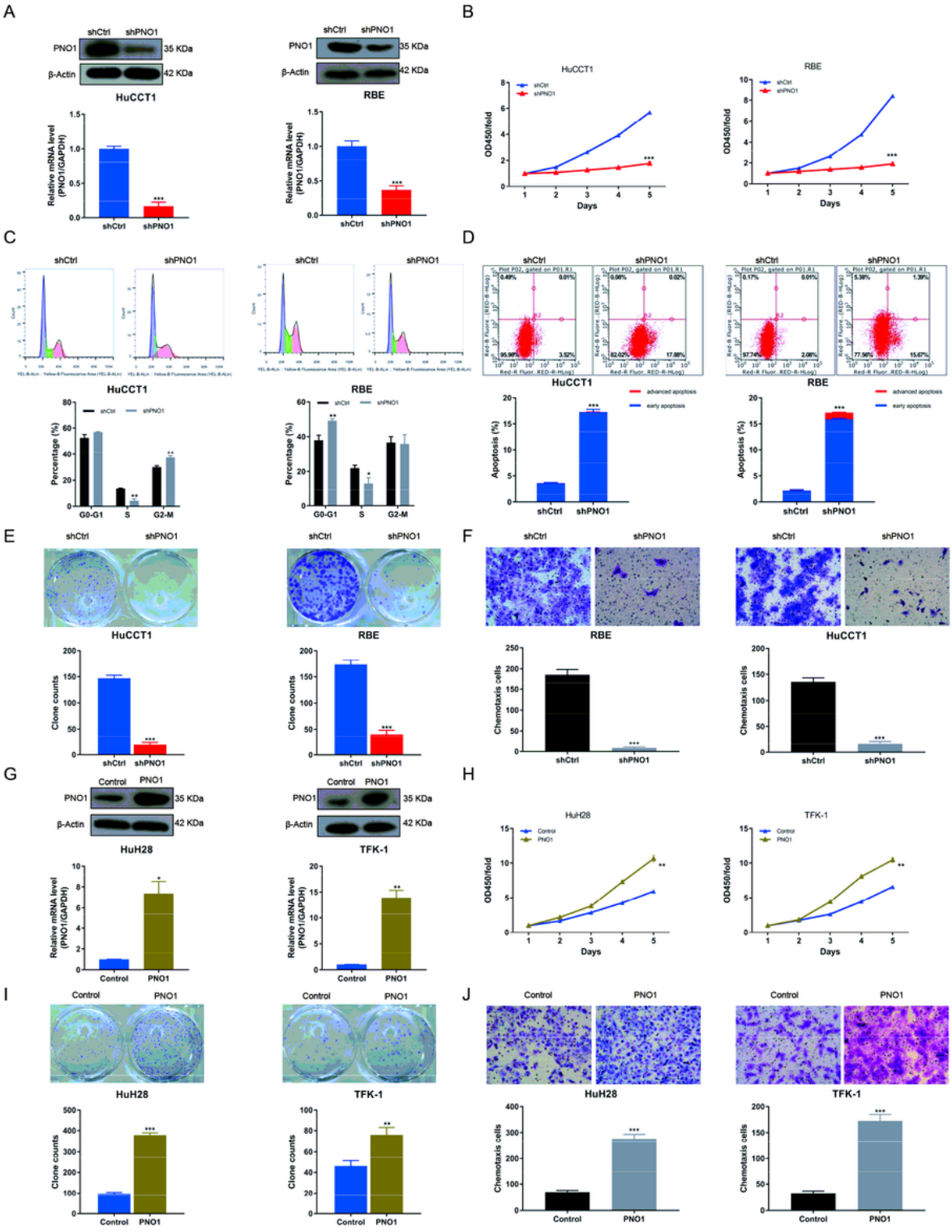

Figure 2

PNO1 promotes CHOL cell proliferation and metastasis in vitro. (A) Western Blotting (upper) and RT-PCR (lower) showing PNO1 protein and mRNA levels in HuCCT1 cells and RBE cells infected with shCtrl or

shPNO1. n=3, ***P<0.001. (B) CCK8 assays showing cell growth in HuCCT1 cells and RBE cells infected with shCtrl or shPNO1. n=3, ***P<0.001. (C) Effects of PNO1 on cell cycle of HuCCT1 cells and RBE cells infected with shCtrl or shPNO1. n=3, *P<0.05, **P<0.01. (D) Effects of PNO1 on cell apoptosis of HuCCT1 cells and RBE cells infected with shCtrl or shPNO1. n=3, ***P<0.001. (E) Plate clone formation assays showing cell proliferation in HuCCT1 cells and RBE cells infected with shCtrl or shPNO1. n=3, ***P<0.001. (F) Transwell assays were used to detect cell migration in HuCCT1 cells and RBE cells infected with shCtrl or shPNO1(50 μm). n=3, ***P<0.001. (G) Western Blotting (upper) and RT-PCR (lower) showing PNO1 protein and mRNA levels in HuH28 cells and TFK-1 cells infected with Control or PNO1(PNO1 overexpression). n=3, *P<0.05, **P<0.01. (H) CCK8 assays showing cell growth in HuH28 cells and TFK-1 cells infected with Control or PNO1(PNO1 overexpression). n=3, **P<0.01. (I) Plate clone formation assays showing cell proliferation in HuH28 cells and TFK-1 cells infected with Control or PNO1(PNO1 overexpression). n=3, **P<0.01, ***P<0.001. (J) Transwell assays were used to detect cell migration in HuH28 cells and TFK-1 cells infected with Control or PNO1(PNO1 overexpression) (50 μm). n=3, ***P<0.001.

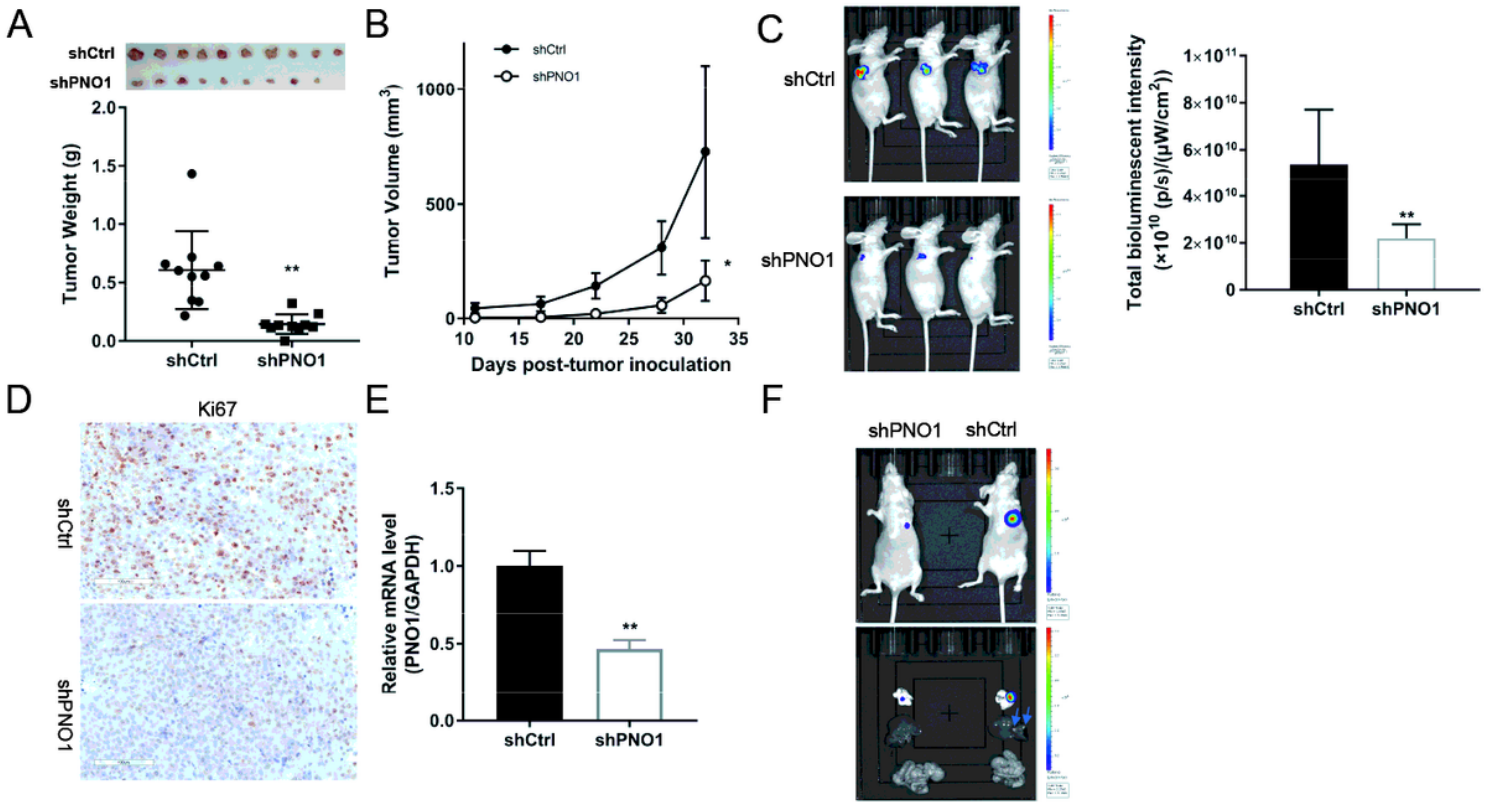

Figure 3

PNO1 knockdown inhibits CHOL tumorigenesis in vivo (A and B) Mice tumor images, weight changes (A) and tumor volume growth curves (B) for subcutaneous xenografts. Images were taken by camara (respectively). n=10, *P<0.05, **P<0.01. (C) Images of the subcutaneous xenografts from the shPNO1 and shCtrl groups. Images were taken by Perkin Elmer IVIS Spectrum (respectively). n=10, *p < 0.05. (D) Representative images of sections sliced from the indicated tumors and stained with anti-Ki67, respectively (100 μm). (E) RT-PCR of PNO1 expression in the indicated tumors. Each bar represents the

mean values ± SD of three independent experiments. n=3, **p < 0.01. (F) Images of the intravenous xenografts from the shPNO1 and shCtrl groups. Images were taken by Perkin Elmer IVIS Spectrum (respectively).

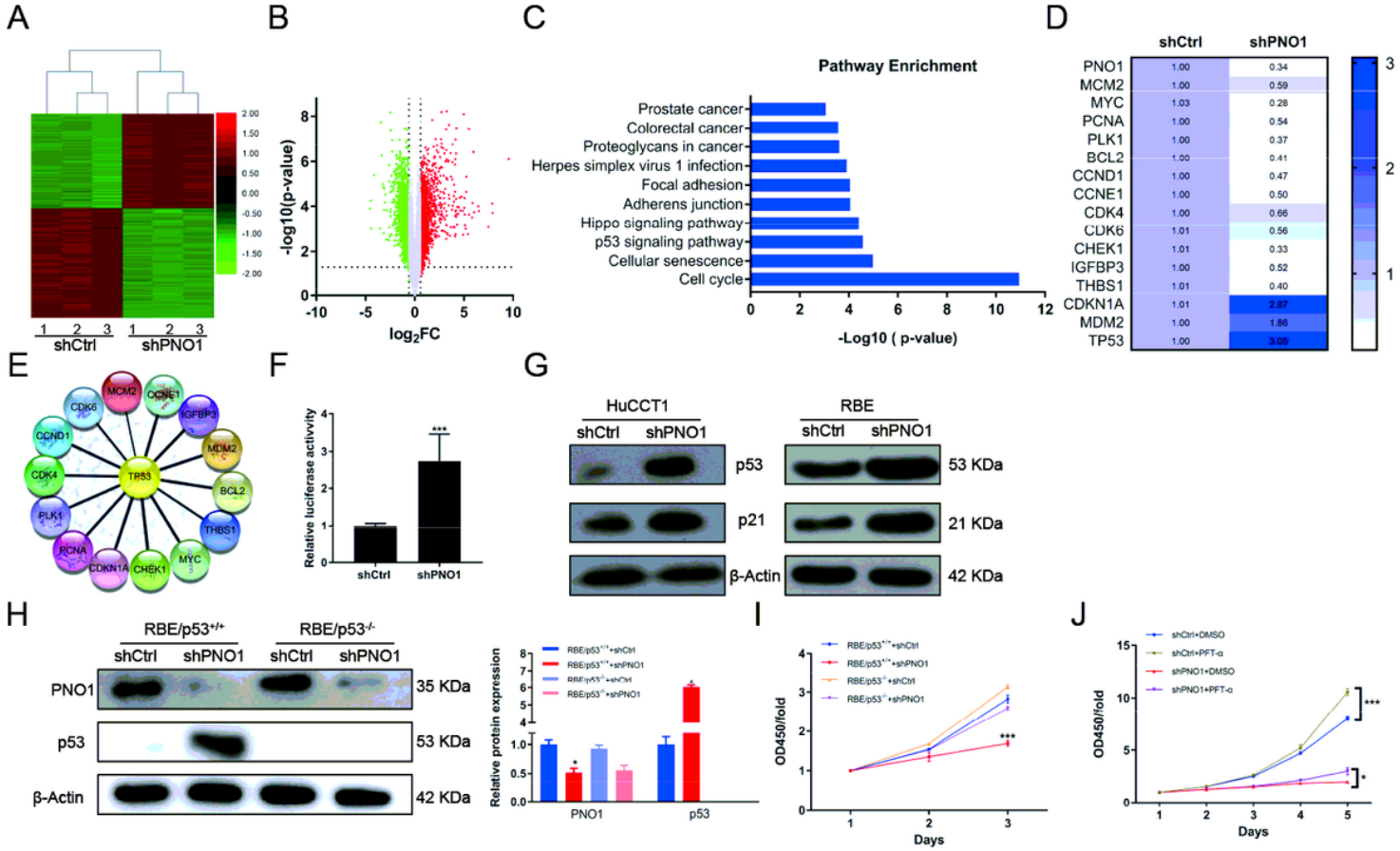

Figure 4

Oncogenic activities of PNO1 depend on p53 signaling (A and B) mRNA microarray analysis was used to identify DEGs in RBE cells infected with shCtrl or shPNO1. A hierarchical clustering plot (A) and a volcano plot (B) were used to identify DEGs (|Fold change| > 1.5, adjusted p-value < 0.05). (C) KEGG Pathway Enrichment Analysis of these DEGs from microarray analysis. (D) RT-PCR showing the intersection DEGs from KEGG Pathway Enrichment Analysis. (E) Network of 15 selected proteins. (F) A dual luciferase assay was performed to determine the effect of PNO1 knockdown on transcriptional activity of TP53 in RBE cells. (G) Western blotting was performed to determine levels of p53 and p21 proteins in both HuCCT1 and RBE cells. (H) RBE/p53+/+ and RBE/p53-/- cells were infected with shCtrl or sh-PNO1, then levels of PNO1 protein were assayed using Western blotting (left). Protein bands were quantitated using ImageJ software and normalized to β-Actin (right). (I) Cell viability was determined using the CCK-8 assay. n=3, ***P<0.001. (J) Cell viability was determined using the CCK-8 assay. RBE cells were infected with shCtrl or sh-PNO1, and treated with PFT-a or not. n=3, *P<0.05, ***P<0.001.

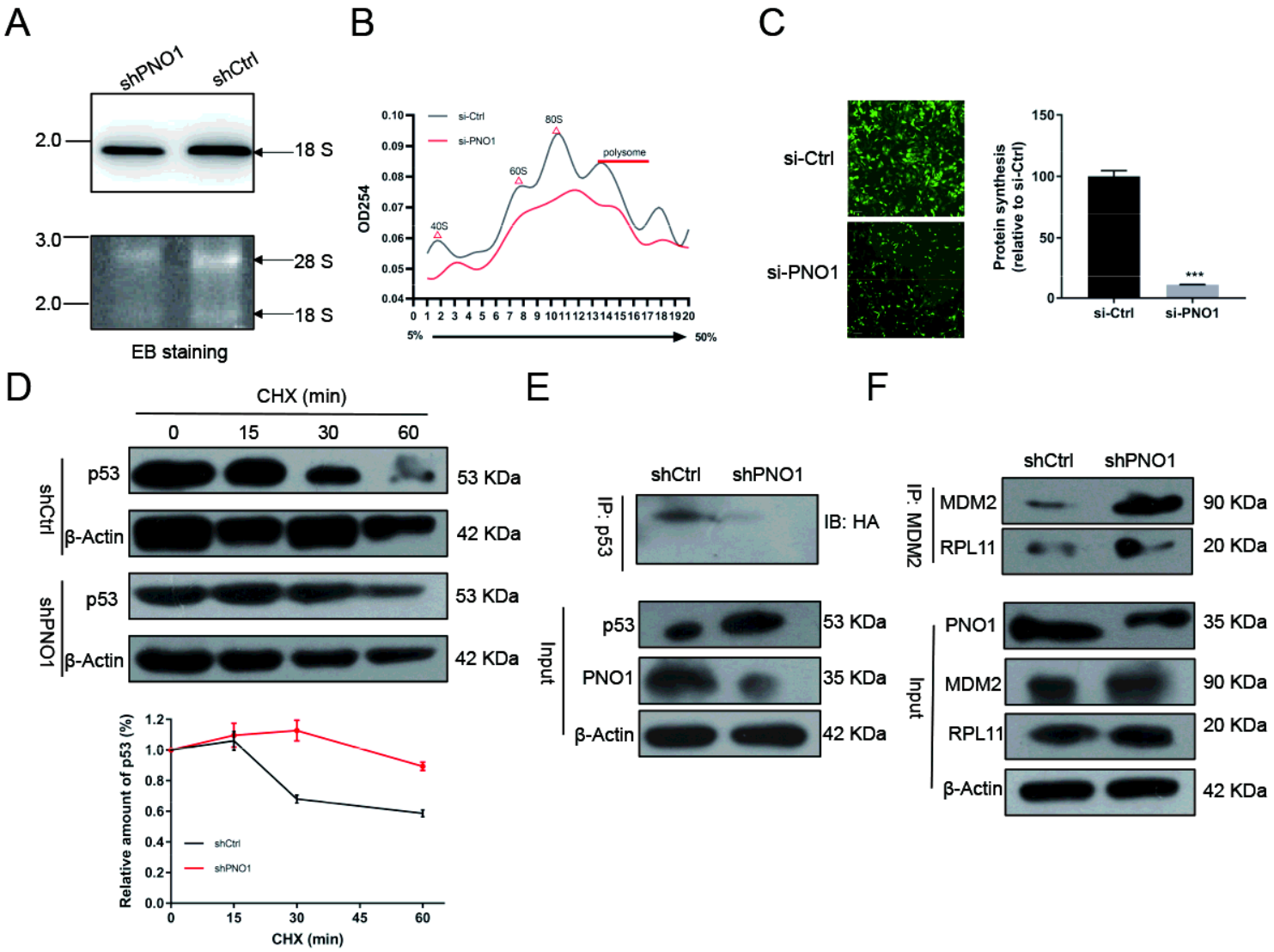

Figure 5

Effects of PNO1 on ribosome biogenesis. (A) 18S rRNA production was detected in RBE cells after PNO1 knockdown using Northern blotting with an 18S rRNA probe. EB, ethidium bromide. (B) Ribosome profiling was performed to determine ribosome biogenesis in RBE cells after PNO1 knockdown. Formation of 40S subunits, 60S subunits, and 80S ribosomes was evaluated by measuring absorbance at 254 nm. (C) Newly synthesized protein was detected in RBE cells after PNO1 knockdown using a protein synthesis assay (50 μm), ***P<0.001. (D) Degradation of p53 was determined by Western blot analysis in RBE cells after PNO1 knockdown, followed by cycloheximide (CHX) treatment or not (top). Amount of p53 was quantified by densitometry and normalized to the level of β-Actin (bottom). (E) Ubiquitination of p53 was determined by Western blot analysis using anti-HA in RBE cells after PNO1 knockdown, followed by transfection with HA-tag overexpressing plasmid. (F) Coimmunoprecipitation (IP) analysis in RBE cells after PNO1 knockdown was performed to determine the binding of RPL11 to MDM2 using anti-MDM2 antibody.

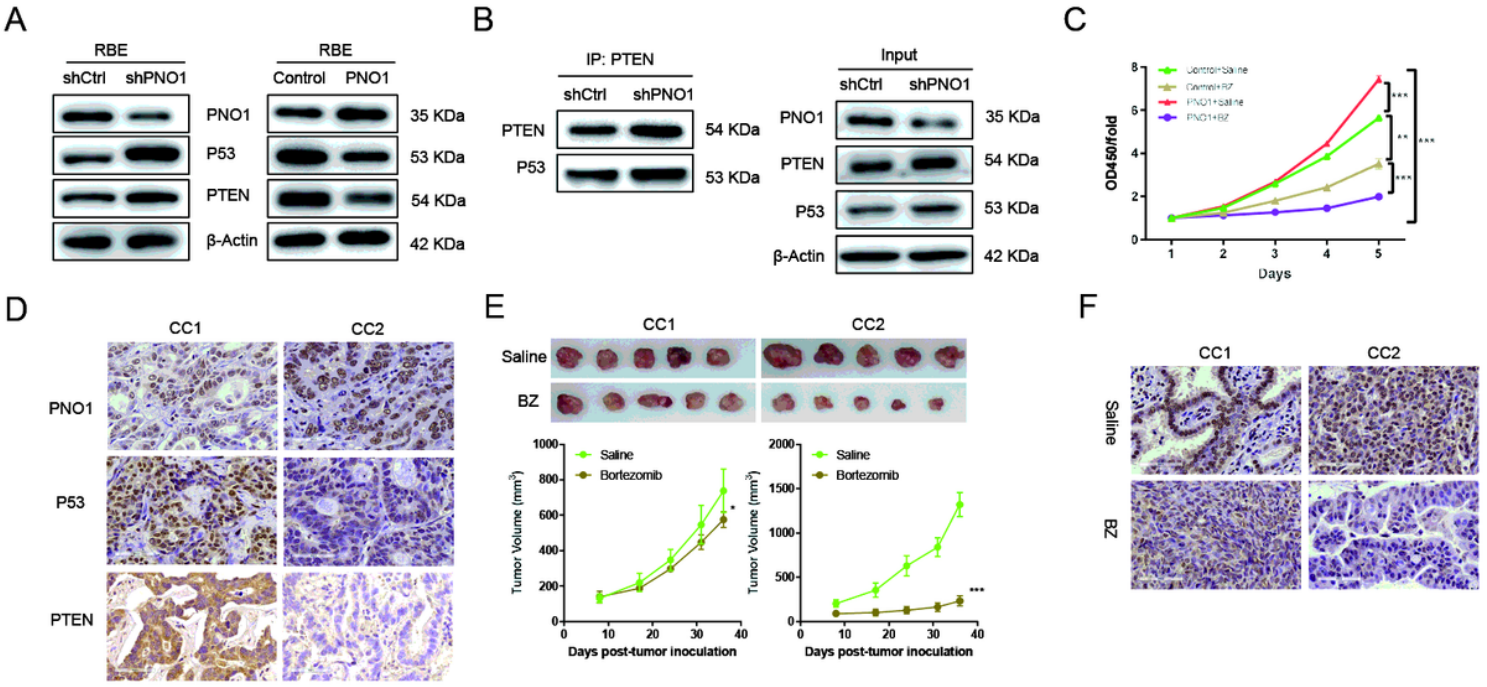

Figure 6

PNO1 facilitates the therapeutic effect of bortezomib in CCA (A) Western Blotting showing PNO1, p53 and PTEN protein levels in RBE cells infected with shCtrl, shPNO1, Control or PNO1. (B) Coimmunoprecipitation (IP) analysis in RBE cells after PNO1 knockdown was performed to determine the binding of p53 to PTEN using anti-PTEN antibody. (C) Cell viability was determined using the CCK-8 assay. RBE cells were infected with Control or PNO1overexpression, and treated with bortezomib or not. n=3, **P<0.01, ***P<0.001. (D) Representative images of PNO1, P53 and PTEN staining in two CHOL samples. Scale bars, 60 μm. (E) Effect of bortezomib treatment on PDX tumor growth. (F) Representative images of Ki67 staining in PDX samples (CC1 and CC2) after treatment with bortezomib or saline. Scale bars, 60 μm.

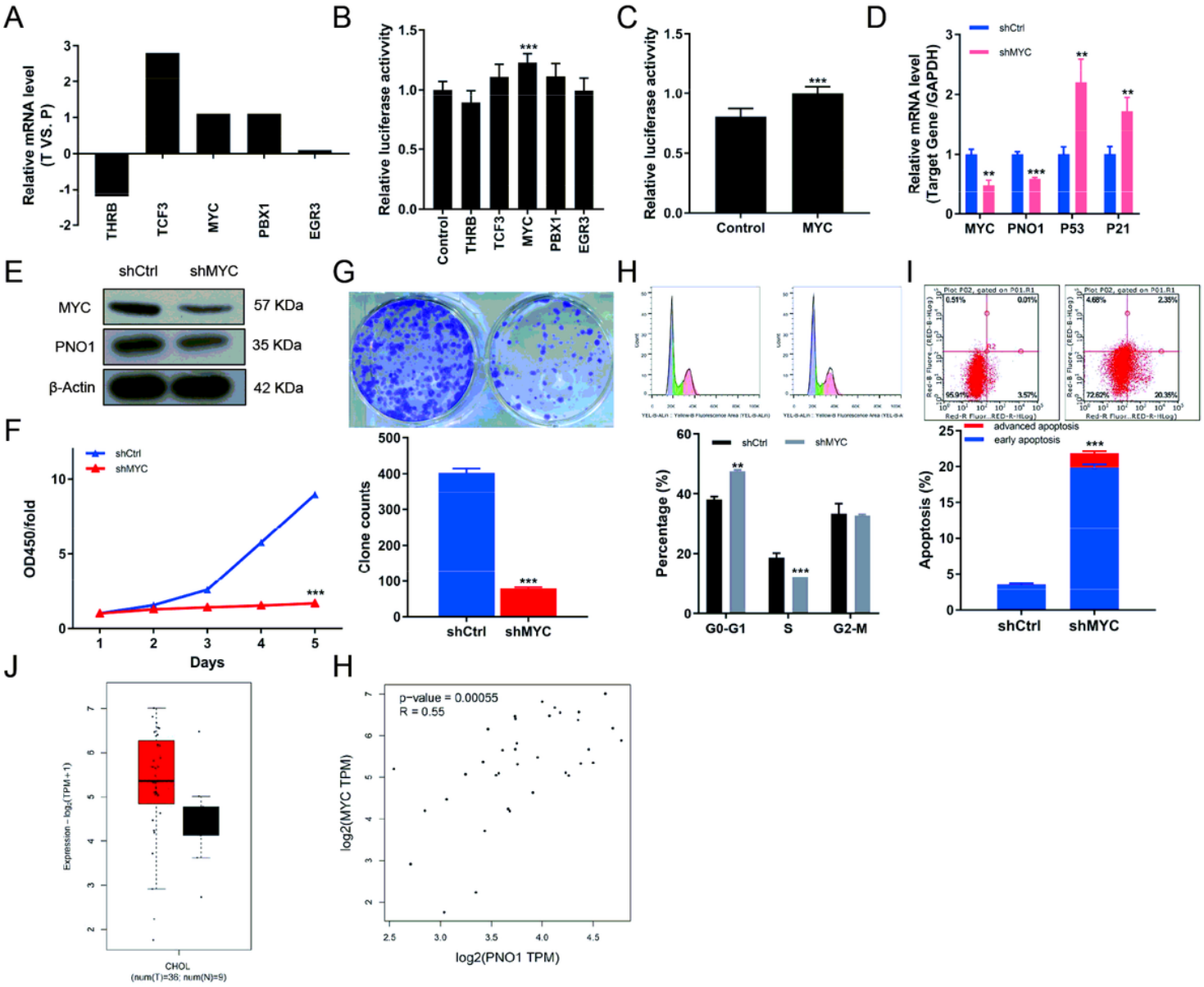

Figure 7

Transcription factor MYC positively regulates PNO1 expression in CHOL (A) The mRNA levels of 5 potential transcription factors between CHOL tissues (T) and para-tumor tissues (P) in mRNA microarray analysis. (B) A dual luciferase assay was performed to assess the effects of 5 potential transcription factors on PNO1 transcription in HEK293T cells, ***P<0.001, versus control. (C) A dual luciferase assay was performed to assess the effects of MYC overexpression on PNO1 transcription in RBE cells, ***P<0.001, versus control. (D) RT-PCR showing indicated mRNA levels in RBE cells infected with shCtrl or shMYC. n=3, **P <0.01, ***P<0.001. (E) Western Blotting showing MYC and PNO1 protein levels in RBE cells infected with shCtrl or shMYC. (F) Effects of MYC on growth of RBE cells infected with shCtrl or shMYC. n=3, ***P<0.001. (G) Effects of MYC on colony formation of RBE cells infected with shCtrl or shMYC. n=3, **P<0.01, ***P<0.001. (H) Effects of MYC on cell cycle of RBE cells infected with shCtrl or shMYC. n=3, ***P<0.001. (I) Effects of MYC on cell apoptosis of RBE cells infected with shCtrl or shMYC. n=3, ***P<0.001. (J) MYC mRNA expression in 36 CHOL tissues and 9 normal tissues were analyzed

using online CHOL database from GEPIA2. *P <0.05. (H) Correlation analysis between the PNO1 mRNA expression and MYC using online CHOL database from GEPIA2.

Supplementary Files

This is a list of supplementary files associated with this preprint. Click to download.

- Fig.S1.tif
- SupplementaryFigurelegends.docx
- SupplementaryTable1.xlsx
- SupplementaryTable2.xlsx
- SupplementaryTable3.xlsx
- SupplementaryTable4.xlsx